

# TeV Gamma-ray Astronomy: A Summary

J. Holder<sup>a</sup>

<sup>a</sup>*Department of Physics and Astronomy and the Bartol Research Institute, University of Delaware, Newark, DE 19716, USA,  
Tel: +(1) 302 831 2545, Fax: +(1) 302 831 1637*

---

## Abstract

The field of TeV gamma-ray astronomy has produced many exciting results over the last decade. Both the source catalogue, and the range of astrophysical questions which can be addressed, continue to expand. This article presents a topical review of the field, with a focus on the observational results of the imaging atmospheric Cherenkov telescope arrays. The results encompass pulsars and their nebulae, supernova remnants, gamma-ray binary systems, star forming regions and starburst and active galaxies.

*Keywords:* Gamma-ray Astronomy, High-energy astrophysics

---

## 1. Introduction

Teraelectronvolt (TeV) astronomy concerns the study of astrophysical sources of gamma-ray photons, with energies in the range between  $\sim 30$  GeV and  $\sim 30$  TeV. The TeV range is one of the most recent windows of the electromagnetic spectrum to be opened for study, beginning with the identification of the first source, the Crab Nebula, in 1989 [1]. The results have been impressive, with significant advances in instrumentation leading to the detection of well over 100 sources over the last decade. The goals of TeV astronomy are wide-ranging, but can broadly be described as the study of sites of relativistic particle acceleration in the Universe, both hadronic and leptonic. This encompasses a huge range of size scales and energetics, from the interactions of galaxy clusters, to the magnetospheres of individual pulsars.

Numerous recent reviews of TeV gamma-ray astronomy have been written (e.g. [2, 3, 4]), but the field is rapidly evolving. For example, since the extensive review by Hinton & Hofmann in 2009 [2], the number of sources has grown from around 80 to more than 120, and a number of new source classes have been identified. This paper therefore aims to provide an update, and to supplement the existing reviews with a summary of the current observational status. The primary focus of the review is on the results from imaging atmospheric Cherenkov telescopes, with a relatively brief discussion

of the air shower particle detector experiments. We use the definitions outlined by Aharonian [5] as follows: “high energy”, or “GeV”, astronomy refers to the energy range from 30 MeV to 30 GeV, while “very high energy”, or “TeV”, astronomy, refers to the range from 30 GeV to 30 TeV.

## 2. A Brief History

The development of ground-based gamma-ray astronomy is closely linked to the study of cosmic rays and cosmic ray air showers. The idea of searching for astrophysical gamma-ray sources at  $\sim 100$  MeV energies was first proposed by Morrison in 1958 [6]. A prediction of a very high TeV gamma-ray flux from various sources, including the Crab, which might be detectable with an air shower particle array at high altitude, was made by Cocconi in 1959 [7]. Cherenkov radiation associated with large cosmic ray air showers was first detected by Galbraith & Jelley in 1953 [8], and the possibility of using this phenomenon to study gamma-ray initiated showers led to the development of a number of dedicated facilities in the 1960s. This effort was boosted by the apparent detection of a gamma-ray signal from the black-hole binary Cygnus X-3 by both particle air shower arrays and atmospheric Cherenkov detectors. With hindsight, this detection was likely spurious, as were numerous unsubstantiated claims throughout the 1970s, 1980s and into the 1990s.

The field reached a firm experimental footing with the development of the imaging technique, which provides

---

*Email address:* jholder@physics.udel.edu ()

a method of effectively discriminating between gamma-ray initiated showers and the background of cosmic ray showers, based on the morphology of their Cherenkov images, and guided by the results of Monte Carlo simulations [9, 10]. This technique was applied by the Whipple collaboration to detect steady gamma-ray emission from the Crab Nebula using a 10m reflector with a 37-element photomultiplier tube camera in 1989 [1]. A number of imaging atmospheric Cherenkov telescopes (IACTs) were subsequently developed around the world (including Durham, CANGAROO, Telescope Array, Crimean Astrophysical Observatory, SHALON, TACTIC), with the northern hemisphere instruments (Whipple, HEGRA and CAT) leading the field. The 1990s saw two particularly important developments: the detection of the first extragalactic sources by the Whipple Collaboration, starting with the nearby blazars Markarian 421 [11] and Markarian 501 [12], and the application of the stereo imaging technique by the HEGRA array [13]. HEGRA consisted of 5 telescopes of modest aperture ( $< 10 \text{ m}^2$ ), and demonstrated that the combination of Cherenkov image information from multiple telescopes located within the same Cherenkov light pool could dramatically improve the sensitivity of the technique.

Despite this progress, the relative scarcity of bright TeV gamma-ray sources ( $< 10$  were identified by 2000) highlighted the necessity for improved instrumentation. Cherenkov wavefront samplers such as CELESTE and STACEE attempted to probe to lower energies, and hence higher gamma-ray fluxes and larger distances, using converted solar farms; however, the difficulty of discriminating gamma-rays from the cosmic ray background using this technique limited its effectiveness. Successful gamma-ray observations using a particle detector were made by the Milagro experiment, which ran from 2000 to 2008, providing a survey of the northern sky with modest sensitivity. Starting with the commissioning of H.E.S.S. in 2003, the new generation of IACTs - H.E.S.S., MAGIC and VERITAS - have provided the required order of magnitude improvement in sensitivity, and firmly established gamma-ray studies as an important astronomical discipline.

### 3. Current Status and Instrumentation

#### 3.1. Imaging Atmospheric Cherenkov Telescopes

The Cherenkov emission from an air shower forms a column of blue light in the sky, with the maximum emission occurring around 10 km above sea level at TeV energies. Cherenkov telescopes used to record these images are essentially rather simple devices, consisting of a

large, segmented optical flux collector used to focus the Cherenkov light onto an array of fast photo-detectors. The optical specifications are not terribly strict; an optical point spread function width of typically  $\sim 0.05^\circ$  is adequate. The photo-detector array (usually  $< 1000$  photomultiplier tubes) comprises a crude camera, covering a few degrees on the sky. A Cherenkov flash triggers read-out of the photo-detectors, with a read-out window defined by the timescale of the arrival of the Cherenkov photons ( $\sim 10 \text{ ns}$ ).

There are currently three major imaging atmospheric Cherenkov telescope systems in operation. H.E.S.S., located in the Khomas Highland of Namibia ( $-23^\circ\text{N}$ ,  $-16^\circ\text{W}$ , altitude 1800 m), consists of four telescopes arranged on a square with 120 m side length. Each telescope has a mirror area of  $107 \text{ m}^2$  and is equipped with a 960 pixel camera covering a  $5^\circ$  field of view. VERITAS, at the Fred Lawrence Whipple Observatory in southern Arizona ( $32^\circ\text{N}$ ,  $111^\circ\text{W}$ , altitude 1275 m) has similar characteristics, with 4 telescopes of  $107 \text{ m}^2$  area and 499-pixel cameras, covering  $3.5^\circ$ . MAGIC ( $28^\circ\text{N}$ ,  $17^\circ\text{W}$ , altitude 2225 m) originally consisted of a single, very large reflector ( $236 \text{ m}^2$ ) on the Canary island of La Palma, with a  $3.5^\circ$  camera. In 2009, a second telescope with the same mirror area was installed at a distance of 85 m from the first.

Each of these facilities work in a similar fashion. Cherenkov images of air showers are recorded at a rate of a few hundred Hz, and analyzed offline. The overwhelming majority of these images are due to cosmic ray initiated air showers. Gamma-ray showers can be discriminated from this background based on the image shape and orientation. Gamma-ray images result from purely electromagnetic cascades and appear as narrow, elongated ellipses in the camera plane. The long axis of the ellipse corresponds to the vertical extension of the air shower, and points back towards the source position in the field of view. If multiple telescopes are used to view the same shower, the source position is simply the intersection point of the various image axes (illustrated schematically in Figure 1). Cosmic-ray primaries produce secondaries with large transverse momenta, which initiate sub-showers. The Cherenkov images of cosmic-ray initiated air showers are consequently wider than those with  $\gamma$ -ray primaries, and form an irregular shape, as opposed to a smooth ellipse. In addition, since the original charged particle has been deflected by galactic magnetic fields before reaching the Earth, cosmic-ray images have no preferred orientation in the camera.

Cherenkov light reaching the ground from air showers peaks at optical/UV wavelengths, and so IACTs operate only under clear, dark skies. Both MAGIC and

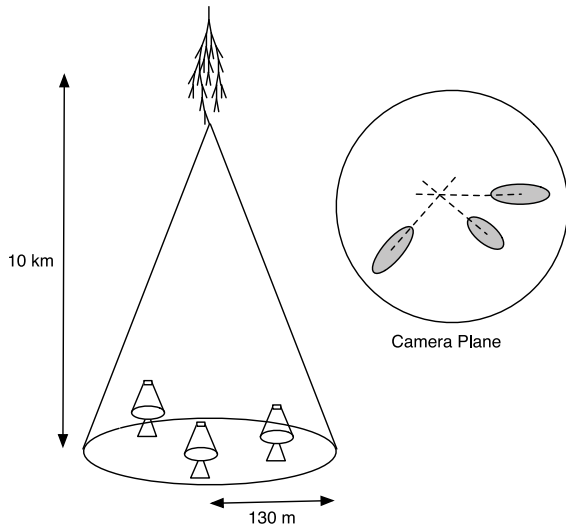


Figure 1: A schematic illustration of an atmospheric Cherenkov telescope array. The primary particle initiates an air shower, resulting in a cone of Cherenkov radiation. Telescopes within the Cherenkov light pool record elliptical images; the intersection of the long axes of these images indicates the arrival direction of the primary, and hence the location of a  $\gamma$ -ray source in the sky.

VERITAS have demonstrated that useful observations can be made when the moon is visible above the horizon, but the typical duty cycle of these instruments is still limited to  $\sim 1200$  hours per year ( $< 15\%$ ). Given the small field of view of IACTs, regions of the sky containing one or more source candidates are usually targeted for observations. Surveys can only be accomplished slowly, by tiling regions of the sky with overlapping fields-of-view. The sensitivity of the current generation of IACTs is sufficient to detect the Crab Nebula in under a minute, and a source with 1% of the Crab flux ( $\sim 2 \times 10^{-13} \text{ m}^{-2} \text{ s}^{-1}$  above 1 TeV) in  $\sim 25$  hours. The angular and energy resolution of the technique are energy-dependent, with typical values of  $< 0.1^\circ$  and  $< 15\%$  per photon, respectively, at 1 TeV.

The catalog of TeV sources grew rapidly with the commissioning of H.E.S.S. in the southern hemisphere, which provided the first high sensitivity observations of the densely populated inner Galaxy. It has continued to expand in recent years as MAGIC and VERITAS have come online, and now numbers 130 sources, as listed in the online catalog *TeVCat* [14]<sup>1</sup>. Figure 2 shows the locations of these sources in Galactic coordinates.

<sup>1</sup>We note that a small fraction of these 130 sources may be duplicate detections of the same object, while other detections remain contentious or unconfirmed. Full details are available in the individual source annotations in *TeVCat*, available at <http://tevcats.uchicago.edu>

### 3.2. Particle Detectors

The direct detection of air shower particles using arrays of particle detectors at ground level offers some important advantages over the atmospheric Cherenkov technique. In particular, observations can be made continuously, both day and night, and over the entire viewable sky (a field-of-view of  $> 1$  steradian). These advantages are offset, however, by the rather low sensitivity to point sources, which is primarily due to the difficulty of rejecting the substantial background of cosmic ray initiated air showers. The angular and energy resolution of these detectors are also significantly worse than IACTs. Early claims for emission from binary systems using sparse particle detector arrays were not confirmed by later, more sensitive instruments (e.g. [15, 16]), indicating the need for a new approach to this problem. Milagro, which operated between 2000 and 2008 in northern New Mexico ( $36^\circ\text{N}$ ,  $107^\circ\text{W}$ ), was the first successful attempt at this.

The Milagro detector consisted of a large water reservoir ( $60 \times 80 \text{ m}$ ) at an altitude of 2630 m, covered with a light-tight barrier, and instrumented with PMTs. The central reservoir provided high-resolution sampling of air shower particles over a relatively small area (compared to the air shower footprint). In 2004 an array of 175 small outrigger tanks were added, irregularly spread over an area of  $200 \times 200 \text{ m}$  around the central reservoir. This configuration, coupled with the development of analysis techniques for cosmic ray background discrimination, provided sufficient sensitivity for the first comprehensive survey of the northern TeV sky. The results showed strong detections of the bright, known TeV sources Markarian 421 and the Crab Nebula, along with the detection of three extended sources in the Galactic plane, each with integrated fluxes comparable to the Crab Nebula at 20 TeV. A few less significant source candidates were also identified in the plane, and a reanalysis following the launch of *Fermi-LAT* also showed fourteen  $3\sigma$  excesses co-located with bright Galactic LAT sources [17]. The Milagro results for the region around the Galactic plane are shown in Figure 3.

Milagro ceased operation in 2008; however, two large particle detector arrays remain in operation at very high altitude in Tibet. ARGO-YBJ is located at 4300 m in Yangbajing, and consists of a single layer of resistive plate chambers completely covering an area of  $110 \times 100 \text{ m}$ . The results of 1265 days of observations were recently presented [19], showing  $> 5\sigma$  detections of the Crab Nebula, Markarian 421 and two Milagro sources. The fact that one of the brightest Milagro

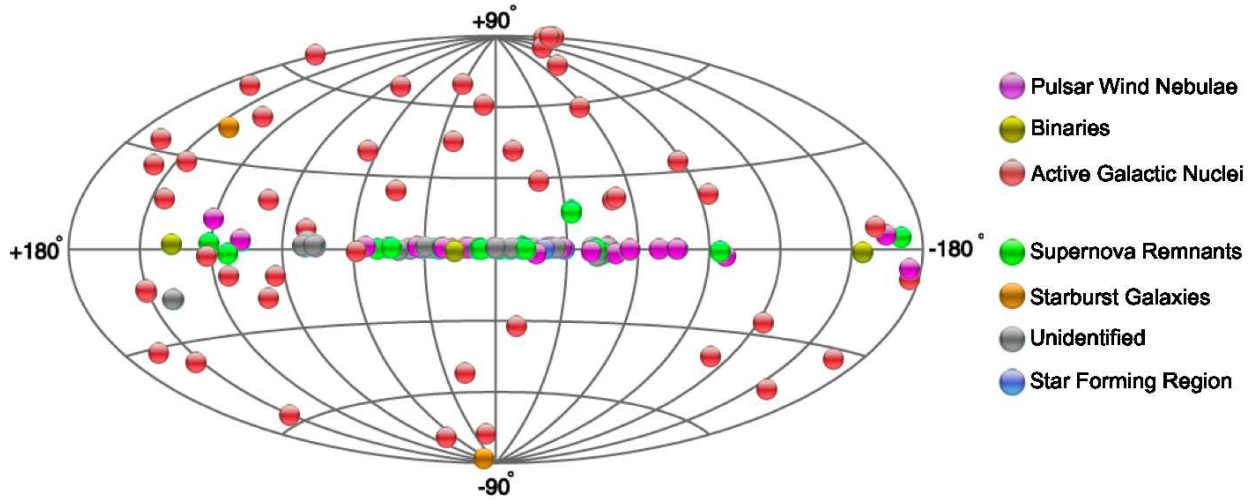


Figure 2: A map of the catalog of localized sources of TeV gamma-ray emission in Galactic coordinates as of November 2011, provided by the online catalog *TeVCat* [14]

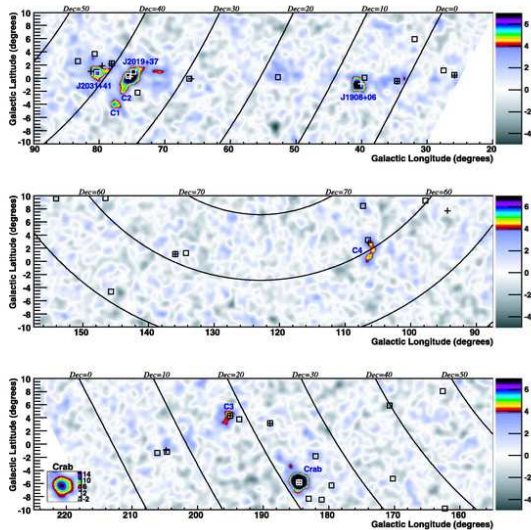


Figure 3: The Milagro survey of the Galactic plane. The  $z$ -axis is the pre-trials statistical significance, with a fixed maximum of  $7\sigma$ . Figure from Abdo et al. [18].

sources, MGRO J2019+37, is not detected in these observations presents something of a mystery. The Tibet AS $\gamma$  air shower array, also at Yangbajing, consists of  $\sim 750$  closely-spaced scintillation detectors covering an area of  $36900 \text{ m}^2$ , and has demonstrated that this technique is also practical for the detection of bright TeV sources [20].

## 4. Extragalactic TeV Sources

### 4.1. Blazars

Approximately 1% of all galaxies host an active nucleus; a central compact region with much higher than normal luminosity. Around 10% of these Active Galactic Nuclei (AGN) exhibit relativistic jets, powered by accretion onto a supermassive black hole. Many of the observational characteristics of AGN can be attributed to the geometry of the system; in particular, the orientation of the jets with respect to the observer. Blazars, which host a jet oriented at an acute angle to the line of sight, are of particular interest for gamma-ray astronomy, as the emission from these objects is dominated by relativistic beaming effects, which dramatically boost the observed photon energies and luminosity.

The first extragalactic source discovered at TeV energies was Markarian 421 [11], a blazar of the BL Lacertae sub-class. The extragalactic TeV catalog now comprises  $\sim 50$  objects, and continues to increase steadily (Figure 4). Blazar SEDs show a double-peaked structure in a  $\nu F_\nu$  representation of their spectral energy distribution (SED), with the lower frequency peak usually attributed to synchrotron emission of energetic electrons, and the higher frequency peak to inverse Compton. BL Lac objects are further classified as low-, intermediate- or high-frequency peaked, according to the location of the peak of their synchrotron emission. The majority ( $\sim 80\%$ ) of the known TeV blazars are high-frequency peaked objects, in part because of inherent biases in the target selection: initially, objects were

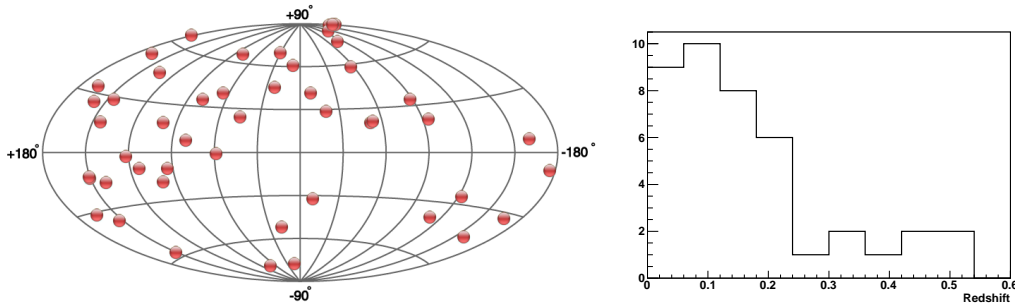


Figure 4: The location of the 49 AGN (BL Lac, FSRQs and radio galaxies) with detected TeV emission (from *TeVCat* [14]). On the left is the spatial distribution, in Galactic coordinates; The right plot shows the redshift distribution, for 41 of the objects with redshifts listed in the literature.

chosen based primarily upon their radio and X-ray spectral properties (e.g. [21]). More recently, the TeV observatories have expanded their selection criteria, using additional guidance in the form of *Fermi*-LAT results, and multi-wavelength observation triggers. This has broadened the catalog to include examples of intermediate- and low-frequency peaked objects. The overall data quality has also improved markedly since the launch of *Fermi*: Figure 5 shows a recent compilation of spectral measurements for the bright TeV blazar, Markarian 501 [22], taken during an extensive multiwavelength campaign in 2009.

The mechanisms which drive the high energy emission from blazars remain poorly understood, and a full discussion is beyond the scope of this review. Briefly; in leptonic scenarios, a population of electrons is accelerated to TeV energies, typically through Fermi acceleration by shocks in the AGN jet. These electrons then cool by radiating X-ray synchrotron photons. TeV emission results from inverse Compton interactions of the electrons with either their self-generated synchrotron photons, or an external photon field. The strong correlation between X-ray and TeV emission which is often observed provides evidence for a common origin such as this, although counter-examples do exist [23]. Another class of models has hadrons as the primary particle population, which can then produce TeV gamma-rays through subsequent interactions with target matter or photon fields. Hadronic models are less favoured, typically, in part because the cooling times for the relevant processes are long, making rapid variability difficult to explain. One exception to this is the case of proton synchrotron emission, which may provide a plausible alternative, in which the emission results from extremely high energy protons in highly magnetized ( $B \sim 100$  G), compact regions of the jet [24].

Many of the AGN detected at TeV energies exhibit extreme variability. The timescales can range from

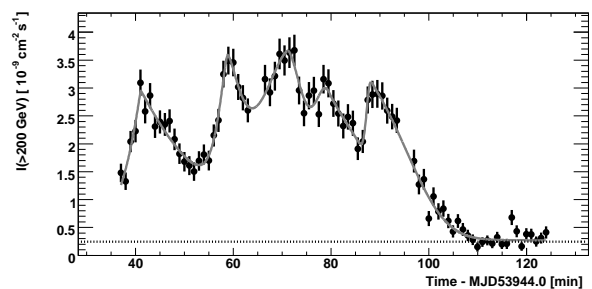


Figure 6: Integrated flux (> 200 GeV) versus time for H.E.S.S. observations of PKS 2155-304 on MJD 53944 (28 July, 2006). The data are binned in 1-minute intervals, and the horizontal dashed line shows the steady flux from the Crab Nebula for comparison. Figure from [29].

years to minutes, and the observed flux can change by more than an order of magnitude. Figure 6 shows the H.E.S.S. lightcurve from July 2006 for one of the most extreme examples, the BL Lac object PKS 2155-304 [18, 25]. Such rapid variability can be used to place constraints on the size of the emission region, which depend upon the Doppler factor,  $\delta$ .  $\delta$  itself is constrained by the requirement that the emission region should be transparent to gamma-rays (e.g. [26]). Extremely rapid TeV gamma-ray variability of distant blazars can also be used to place limits on the energy-dependent violation of Lorentz invariance [27, 28], as predicted in some models of quantum gravity.

Related to the BL Lacertae objects are Flat Spectrum Radio Quasars (FSRQs). These are characterized primarily by their intense UV emission, associated with an accretion disk, strong broad emission lines in the optical spectrum, and infra-red emission associated with a dusty torus. FSRQs are similar to low-frequency peaked BL Lacs, in that the X-ray emission is dominated by the inverse Compton peak of the SED. Despite this, inverse Compton emission can extend up to TeV ener-



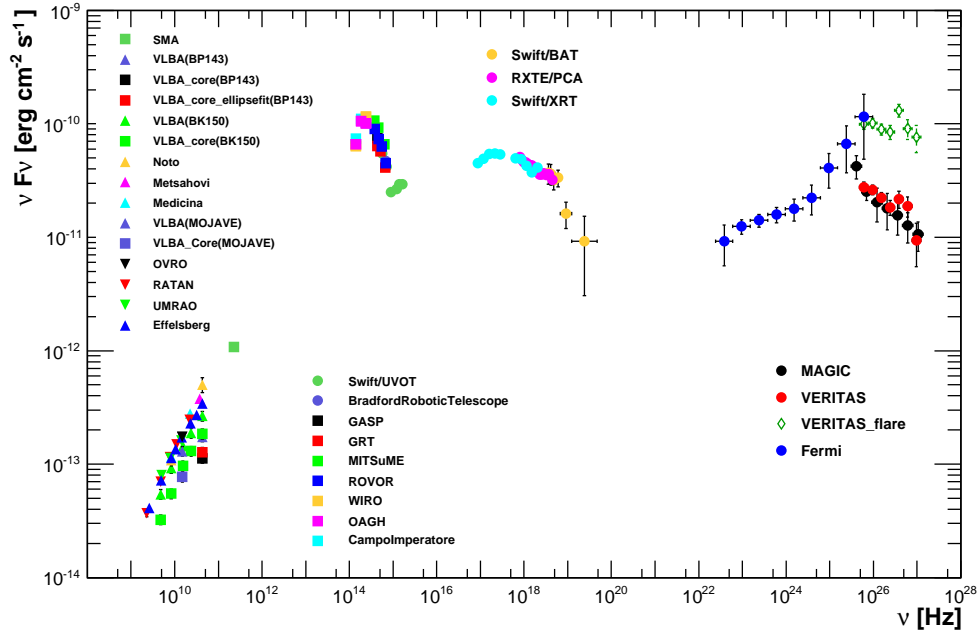


Figure 5: Extensive multifrequency measurements showing the spectral energy distribution of Markarian 501 for observations in 2009. Emission from the host galaxy is clearly visible at infrared/optical frequencies. The VERITAS data are divided to show both the average spectrum (red circles), and the spectrum during a 3-day flare (green triangles). Figure from Abdo et al. [22]

gies, particularly during intense flaring episodes, and three FSRQs have recently been detected by IACTs (PKS 222+21 [30], PKS 1510-089 [31] and 3C279 [32]).

A unique additional case is the TeV detection of IC 310, a “head-tail” radio galaxy in the Perseus cluster, possibly hosting a low-luminosity BL Lac nucleus [33]. Head-tail radio galaxies display a distinctive radio morphology, consisting of a bright “head” and a fainter “tail”, which is believed to be the result of their rapid motion with respect to the intracluster medium. The source was originally identified as a VHE emitter in an analysis of the highest energy ( $> 30$  GeV) Fermi photons by Neronov et al. [34], and then subsequently detected from the ground by MAGIC [35]. Neronov et al. considered the intriguing possibility that the emission might originate with particles accelerated at the bow shock formed by the interaction between the relativistic outflow from the galaxy and the intracluster medium. This scenario is ruled out by the detection of variability in the TeV flux by MAGIC, and the more familiar BL Lac mechanisms are now favoured.

Figure 4 also shows the distribution of measured redshifts for 41 TeV AGN. Some of these measurements are rather uncertain, since BL Lac optical spectra, by definition, do not contain strong emission lines. The

most distant object detected is 3C279 [32], with a relatively modest redshift of  $z = 0.5362$ . The population is truncated at large distances due to the absorption of TeV gamma-rays by electron-positron pair production with the low energy photons of the extragalactic background light (EBL). This effect is energy dependent, and can strongly modify the observed VHE spectra of extragalactic sources. While this limits the observation of more distant TeV sources, it also provides a mechanism by which to infer the intensity of the EBL, using reasonable assumptions about the intrinsic TeV spectra at the source [36]. The EBL provides a calorimetric measure of the complete history of star and galaxy formation in the Universe, but is difficult to measure directly, due to the presence of bright local foreground sources of emission, such as zodiacal light. Presently, all of the TeV blazar measurements are consistent with a relatively low level of EBL, with the constraints derived from VHE measurements now approaching the lower limits derived from galaxy counts [37, 38, 39].

TeV blazar observations have also been suggested as probes of other physical phenomena, such as the acceleration and propagation of ultra-high energy cosmic rays [40, 41], or, more speculatively, the production of axion-like particles [42, 43]. Various authors have also discussed the possibility that TeV observations may be

used to measure or constrain the strength of the intergalactic magnetic field (IGMF) (e.g. [40, 44]). Temporal, spectral and spatial signatures of the IGMF are all possible; however, the fact that blazars are intrinsically variable gamma-ray sources limits the power of this technique. Accounting for this, Dermer et al. derive a lower limit of  $B_{IGMF} \geq 10^{-18}$  G [45].

#### 4.2. Radio Galaxies

As described above, the TeV fluxes from blazars are dramatically enhanced by the effects of Doppler boosting. Nearby radio galaxies, in which the jet is not directly oriented towards the line-of-sight, provide an alternative method by which to investigate the particle acceleration and gamma-ray emission from relativistic outflows in AGN. The advantage of studying such objects lies in the fact that the jets can be resolved from radio to X-ray wavelengths, allowing the possibility of correlating the gamma-ray emission state with observed changes in the jet structure. Three radio galaxies have been identified as TeV emitters: M 87, Centaurus A and NGC 1275.

M 87 is the most well studied of these, and was first reported as a gamma-ray source by the HEGRA collaboration [46], with subsequent confirmation by H.E.S.S. [47], VERITAS [48] and MAGIC [49]. M 87 is a giant radio galaxy at a distance of  $16.7 \pm 0.2$  Mpc, displaying a prominent misaligned jet, with an orientation angle of  $\leq 20^\circ$  to the line-of-sight. The mass of the central black hole is estimated to be  $\sim 3 \times 10^9 M_\odot$ . The TeV source is strongly variable, and has undergone three episodes of enhanced emission in 2005, 2008 and 2010 (Figure 7). The results are summarized by Abramowski et al [50]. Causality arguments use the shortest variability timescale of around 1 day to place strong constraints on the size of the TeV emission region, corresponding to only a few Schwarzschild radii. The TeV emission region cannot be directly resolved with IACTs, but correlations with contemporaneous X-ray and radio observations provide some clues to its location. Two structures are of particular interest: the inner region close to the central black hole (the “core”), and HST-1, a bright jet feature first resolved in the optical band by the *Hubble Space Telescope*. HST-1 underwent a multi-year flare in radio, optical and X-rays, peaking around the time when the first short-term variability was detected at VHE energies [47]. In contrast to this, the 2008 VHE flare was accompanied by enhanced radio and X-ray fluxes from the core region [51]. The 2010 VHE flare showed no enhanced radio emission from the core, although an enhanced X-ray flux was observed 3 days after the VHE

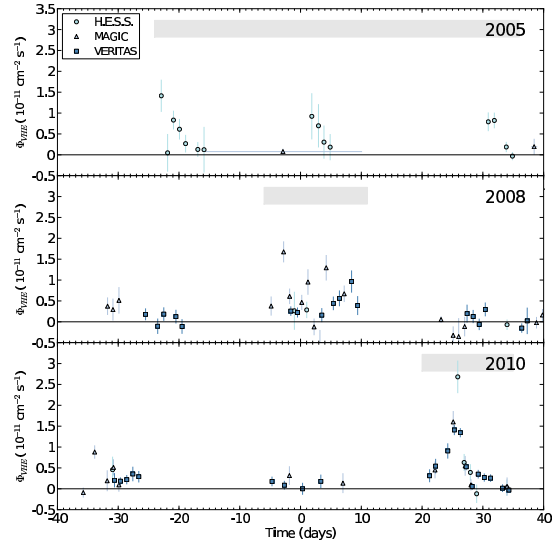


Figure 7: VHE light curves of the three flares from M87 observed in 2005, 2008 and 2010, showing integral fluxes above an energy of 350 GeV. Figure from [50].

peak. The results, therefore, remain somewhat ambiguous, and the possibility remains that the observed VHE flares may have different origins, or that the total VHE emission may be the sum of multiple components. Given the burdensome observing requirements for instruments with a limited duty cycle, M 87 represents the best example of the importance of data-sharing and coordinated observing planning between the various IACTs.

The closest active galaxy, Centaurus A, at a distance of 3.8 Mpc, was identified as a VHE source in a deep, 120 hour exposure by H.E.S.S. [52]. Cen A is among the faintest VHE sources detected, with a flux of 0.8% of the Crab Nebula above 250 GeV. The emission is steady, although the variability is not strongly constrained as a result of the low flux level. As with M 87, numerous sites for the production of the TeV emission have been suggested, from the immediate vicinity of the central black hole (with a mass of  $\sim 5 \times 10^7 M_\odot$ ), to the AGN jet, or even beyond [53]. The final, and most recent, addition to the known TeV radio galaxies is NGC 1275, identified by MAGIC [54]. NGC 1275 is the central galaxy of the Perseus cluster, at a distance of 72.2 Mpc. The VHE emission has a flux of  $\sim 3\%$  of the Crab Nebula above 100 GeV and exhibits a very soft spectrum, with a power-law index of  $3.96 \pm 0.37$  [55], indicating a sharp turnover from the measured Fermi spectrum at lower energies, where the index is

$2.09 \pm 0.02$  [56].

#### 4.3. Starburst Galaxies

Starburst galaxies are those which exhibit an extremely high rate of star formation, sometimes triggered by interaction with another galaxy. High cosmic-ray and gas densities in the starburst region make these objects promising targets for gamma-ray observations, with emission predicted to result from the interactions of hadronic cosmic rays in the dense gas. TeV emission has now been identified from two starburst galaxies: M 82 [57] and NGC 253 [58].

M 82 is a bright galaxy located at a distance of approximately 3.9 Mpc, with an active starburst region at its centre. The star formation rate in this region is approximately 10 times that of the Milky Way, with an estimated supernova rate of 0.1 to 0.3 per year. A deep VERITAS exposure (137 hours) in 2008-2009 resulted in a detection of gamma-ray emission from M 82 with a flux of  $(3.7 \pm 0.8_{stat} \pm 0.7_{syst}) \times 10^{-13} \text{ cm}^{-2} \text{ s}^{-1}$  above the 700 GeV energy threshold of the analysis. NGC 253 lies at a distance of 2.9 – 3.6 Mpc, and also has a central, compact ( $\sim 100$  pc) starburst region. The supernova rate in this region is estimated at  $\sim 0.03$  per year. TeV emission was detected by H.E.S.S. with an integrated flux above 220 GeV of  $(5.5 \pm 1.0_{stat} \pm 2.8_{syst}) \times 10^{-13} \text{ cm}^{-2} \text{ s}^{-1}$  [58].

The emission from both M 82 and NGC 253 is consistent with the predictions of models based on the acceleration and propagation of cosmic rays in the starburst core (e.g. [59]), assuming that they act as efficient “proton calorimeters” (i.e. cosmic rays lose the majority of their energy to collisions). In this case, the estimated cosmic ray density in the starburst region is 2-3 orders of magnitude larger than that of the Milky Way. An alternative explanation is proposed by Mannheim et al. [60], who suggest that the TeV luminosity is consistent with the combined emission from a large population of pulsar wind nebulae, which result from the elevated supernova rate. More accurate TeV spectra, and observation of other starburst classes, such as ultra-luminous infrared galaxies, should provide more insight in the future.

#### 4.4. The Large Magellenic Cloud

Galaxies of the Local Group are also of interest to TeV observatories, although the predicted fluxes due to cosmic ray acceleration and propagation lie below the current instrumental sensitivity in the TeV range. Given

their proximity, the possibility arises of detectable emission from individual objects, or from localized regions, particularly in the Milky Way’s satellite galaxies. H.E.S.S. has recently identified the first such object in the Large Magellenic Cloud (LMC), at a distance of 48 kpc [61]. An unresolved source with a flux of  $\sim 2\%$  of the Crab Nebula ( $1.5 \times 10^{-12} \text{ erg cm}^{-2} \text{ s}^{-1}$  between 1 and 10 TeV) was detected, consistent with the location of PSR J0357-6910. This object is the most powerful pulsar known, with a spin-down energy of  $\dot{E} = 4.8 \times 10^{38} \text{ erg s}^{-1}$ . Given the positional coincidence, and based on comparisons with similar objects within our Galaxy, it seems likely that the TeV emission is due to inverse Compton emission from electrons in the pulsar’s wind nebula interacting with a strong infrared target photon field. This is in contrast to the extended GeV emission which has been observed from the LMC by *Fermi*-LAT, which is attributed to cosmic ray acceleration and interactions in the massive star forming region of 30 Doradus [62].

#### 4.5. Other Extragalactic TeV targets

TeV observations have also been used to place important constraints on the gamma-ray emission from numerous undetected extragalactic source classes, including galaxy clusters and potential sources of ultra-high energy cosmic rays. Here we summarize two of the most important: gamma-ray bursts, and the predicted sites of dense regions of dark matter particles.

**Gamma-Ray Bursts:** GRBs are the signatures of brief, extremely energetic explosions which occur at cosmological distances. They are observationally divided into short and long classes, which are presumably the result of different progenitor systems. Long duration GRBs are generally ascribed to the collapse of massive, rapidly rotating stars into black holes. The origin of the short bursts is less certain, although neutron star - neutron star merger events are among the favoured candidates. The search for  $> 100$  GeV emission has been a long-running goal of both the IACTs and particle detectors (see [63] for a review). Given the brief duration of GRB emission, the wide field-of-view of particle detectors is particularly important in this regard, although observations so far have been hampered by limited sensitivity. IACTs, conversely, must be re-pointed rapidly on receipt of an alert. The detection of delayed high energy emission by *Fermi*-LAT, lasting hundreds to thousands of seconds longer than the sub-MeV emission, has provided additional impetus to the search [64, 65], and IACTs now regularly target burst locations within  $< 100$  s of the burst alert. The task is difficult, since the burst must also be at a small enough redshift such



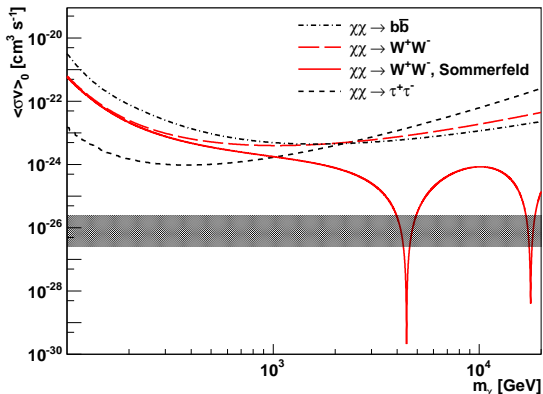


Figure 8: Upper limits at the 95% confidence level on the velocity-weighted annihilation neutralino cross-section for different annihilation channels, based on VERITAS observations of the Segue I dwarf spheroidal galaxy. The dark band represents the typical range of predictions. Figure from [73]

that the high energy emission is not completely suppressed by photon-photon pair production ( $z \lesssim 0.5$ ). No convincing signals have been detected as yet (e.g. [66, 67, 68, 69]), although predictions based on the brightest bursts observed by the LAT indicate that the potential for detecting TeV emission associated with a GRB is promising, assuming no intrinsic spectral cut-off of the high energy emission [70].

**Extragalactic Dark Matter:** The search for the self-annihilation signature of dark matter particles in astrophysical objects is wide-ranging, and complementary to direct detection techniques on the Earth (see [71] for an excellent review). As discussed later in this review, the centre of our own Galaxy is a natural target for dark matter searches, and provides the most stringent limits to date [72]. Objects outside of our own Galaxy are also worthy of investigation, however, and are potentially much less affected by contamination from unknown astrophysical background sources (supernova remnants, pulsar wind nebulae, etc.). Dwarf spheroidal galaxies of the local group are among the most promising of these, due to their proximity and their presumed large dark matter content. The Sloan Digital Sky Survey has more than doubled the known population of dwarf spheroidals, providing additional targets for the TeV searches. No signals have been detected as yet, despite deep exposures on a number of objects [73, 74, 75, 76, 77]. Figure 8 shows upper limits on the annihilation cross-section derived for various annihilation channels using VERITAS observations of the Segue I dwarf spheroidal.

## 5. Galactic TeV Sources

There are presently  $\sim 80$  known TeV sources within our Galaxy, as indicated either by their association with known Galactic sources at other wavelengths, or by their location in the Galactic plane - a particularly compelling argument when coupled with a resolvable angular extent. The majority of these sources were identified as TeV emitters during the H.E.S.S. survey of the inner Galaxy [78]. H.E.S.S. is the only IACT currently operating in the southern hemisphere, which allows it to view the inner Galaxy at high elevation, and hence with a low energy threshold and good sensitivity. H.E.S.S. was the first instrument with sufficient sensitivity to observe sources with  $\lesssim 10\%$  of the Crab Nebula flux in this region, and the results have been revelatory - the Galactic plane is densely populated with TeV sources, primarily clustered within the inner  $\pm 60^\circ$  in Galactic longitude (Figure 9). The most recent survey results consist of 2300 hours of observations, allowing the detection of over 50 sources within the range  $l = 280^\circ$  to  $60^\circ$  and  $b = -3.5^\circ$  to  $+3.5^\circ$  [79]. Observations of the outer Galactic regions by VERITAS, MAGIC, Milagro and ARGO-YBJ have revealed a less densely populated sky, but containing some unique objects of particular interest for TeV studies. Many Galactic TeV sources are extended, allowing detailed studies of source morphology and spatially resolved spectra, while others are time variable and/or periodic. The various source classes are discussed in some detail below.

### 5.1. The Galactic Centre and Ridge

A TeV source at the location of the Galactic Centre has been reported by various IACTs [80, 81, 82, 83]. Determining the nature of this source is a difficult task, due to the complexity of the region, which includes multiple different potential counterparts. The most detailed studies have been performed by H.E.S.S., which reveal that the emission is dominated by a bright central source, HESS J1745-290, lying close to the central supermassive black hole, Sgr A\*. An additional, fainter, component is also seen, which extends in both directions along the Galactic plane [84]. The extended component is spatially correlated with a complex of giant molecular clouds in the central 200 pc of the Milky Way, and the TeV emission can be attributed to the decay of neutral pions produced in the interactions of hadronic cosmic rays with material in the clouds. The central source is point-like, steady and exhibits a curved power-law spectrum [85]. Its location with respect to three of the most likely counterparts is shown in Figure 10. This study reveals that the source centroid is

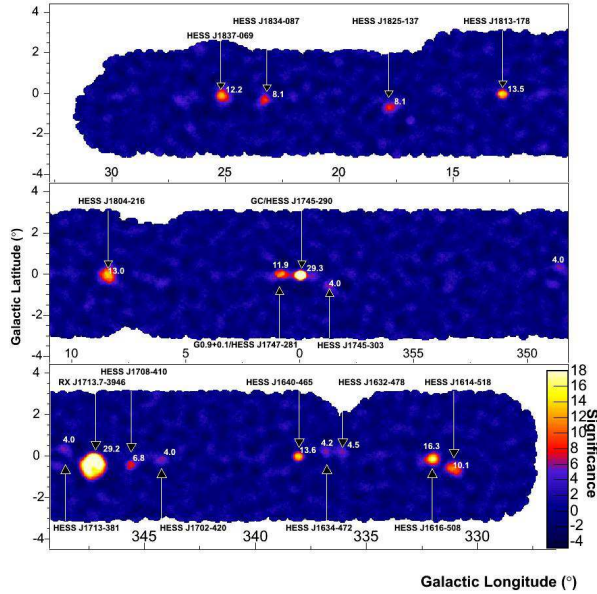


Figure 9: Significance map of the Galactic Plane from the original H.E.S.S. survey in 2004, based on 230 hours of observations. The complete survey now extends over the range from  $l = 280^\circ$  to  $60^\circ$  and  $b = -3.5^\circ$  to  $+3.5^\circ$ , and comprises 2300 hours of observations [79]. Figure from [78]

displaced from the radio centroid of the supernova remnant Sgr A East, excluding this object with high probability as the dominant source of the VHE gamma-ray emission, and leaving Sgr A\* and the pulsar wind nebula G359.95-0.04 as the most likely counterparts [86].

The Galactic Centre is also a prime candidate region in which to search for gamma-ray emission due to dark matter particle self-annihilation. The analysis is complicated, however, because of the high background due to astrophysical sources. An analysis by H.E.S.S. using an optimized background subtraction technique shows no hint of a residual dark matter gamma-ray flux at a projected distance of  $r \sim 45 - 150$  pc from the Galactic Centre [72].

### 5.2. The Crab Nebula and Pulsar

The Crab is the nearby ( $2.0 \pm 0.2$  kpc) remnant of a historical supernova explosion, observed in 1054 A.D. There is no detected shell, and the broadband emission below  $\sim 100$  MeV is dominated by a bright synchrotron nebula, powered by a central pulsar (PSR B0531+21). PSR B0531+21 is the most energetic pulsar in our Galaxy, with a pulse period of 33 ms, and a spin-down power of  $4.6 \times 10^{38}$  erg  $s^{-1}$ . The Crab Nebula and Pulsar hold a unique place in the development of TeV astronomy: the birth of the field as an astronomical disci-

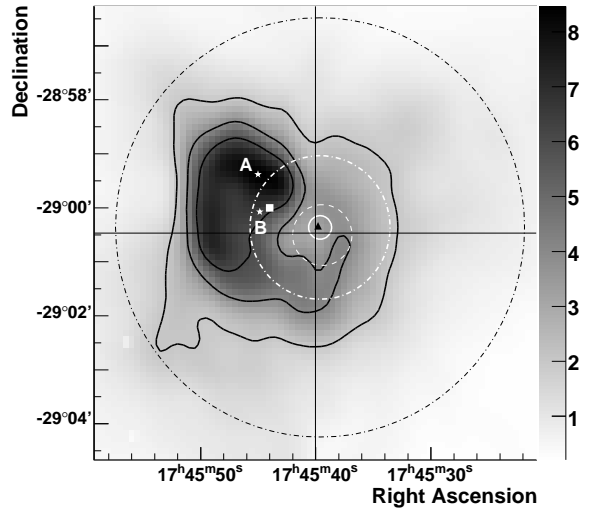


Figure 10: 90 cm VLA radio flux density map of the innermost 20 pc of the Galactic Centre, showing emission from the SNR Sgr A East. Black contours denote radio flux levels; the centre of the SNR is marked by the white square, and the positions of Sgr A\* and G359.95-0.04 are given by the cross hairs and the black triangle, respectively. The 68% CL total error contour of the best-fit centroid position of HESS J1745-290 is given by the white circle. Figure from [86]: see that paper for full details.

pline can be traced to the detection of the Crab Nebula TeV source by Weekes et al. using the Whipple 10 m telescope, in the first application of the imaging atmospheric Cherenkov technique [1]. Subsequently, the Crab has acted as a bright, standard candle for TeV observatories.

The SED of the non-thermal nebula emission displays two components (Figure 11). The dominant, low frequency component is explained by synchrotron radiation of high energy electrons spiraling in the magnetic field of the nebula [87, 88]. The higher frequency component is attributed to inverse Compton scattering of lower energy photons by these electrons, including microwave background photons, far infrared and the electron-synchrotron photons themselves. The electron population reaches energies of at least  $10^{15}$  eV, through acceleration occurring both in a relativistic particle outflow driven by the spin-down energy of the pulsar, and in shocks where this outflow encounters the surrounding nebula. The highest energy particles likely require an alternative explanation for their origin, such as direct acceleration in intense electric fields associated with the pulsar itself [89]. Observations of the synchrotron nebula from radio to X-ray wavelengths provide high resolution imaging of the emission region; however, the syn-

chrotron data alone only contain information concerning the product of the magnetic field strength and the relativistic electron density. Since the inverse Compton component is independent of the magnetic field strength, the combined SED allows an estimate of the Nebula magnetic field, which is now constrained to be between 100 and 200  $\mu\text{G}$  [90].

The search for a VHE component to the pulsed emission from the Crab has been long and, until recently, fruitless. Despite discouraging model predictions, and the detection of spectral cut-offs below 10 GeV in other pulsars, the fact that no super-exponential cut-off was observed by EGRET in the Crab Pulsar spectrum initially provided some encouragement for a continued search by IACTs [91]. *Fermi*-LAT subsequently extended the GeV spectrum and measured a sharp spectral cut-off at 6 GeV [90]. A campaign by MAGIC, using a specially designed “analog sum” hardware trigger, provided the first ground-based measurement of gamma-ray emission from the Crab pulsar [92]. The initial MAGIC flux measurement above 25 GeV was, like the *Fermi*-LAT result, consistent with an exponential cut-off. The existence of an exponential cut-off is a natural consequence of emission due to curvature radiation, as favored by various models (e.g. [93]). Both VERITAS and MAGIC recently presented new results, which challenge this paradigm [94, 95, 96]. Pulsed emission is observed to extend up to well beyond 100 GeV, and the combined LAT-IACT spectrum can best be fit with a broken power law. The explanation for this high energy component is an open question, at present. Gamma-ray opacity arguments require that the emission zone of the highest energy photons must be at least 10 stellar radii from the surface of the neutron star - much further than previously assumed. The results require either a substantial revision of existing models of high energy pulsar emission, or the addition of a new component, not directly related to the MeV-GeV emission.

As mentioned above, the Crab has been used as a standard candle in TeV astronomy, on the assumption that its emission was steady. This is now demonstrably false, at least at energies below  $\sim 1$  GeV, with the detection of multiple day-scale flaring events [98, 89], and long term variation in the hard X-ray/ soft gamma-ray regime [99]. The GeV spectrum during flares indicates that the emission is confined to the synchrotron component of the SED, a conclusion which is supported by the rapid timescale of the events (since the inverse Compton or Bremsstrahlung cooling time of the emitting electrons is much greater than the observed flare duration). At higher energies, some evidence for an enhanced flux during HE flare states has been presented by

ARGO-YBJ [100]. IACT measurements do not support these results, but are not necessarily in conflict, given the differing duty cycles. Detailed measurements with IACTs during future flare states are required to resolve this question.

### 5.3. Pulsar Wind Nebulae

Pulsar wind nebulae are the most abundant class of known VHE emitters in the Galaxy, with  $\sim 30$  firm examples, and numerous other sources where the PWN association is more tentative (for reviews see e.g. [101, 102, 103]). The essential emission mechanisms - shock accelerated leptons producing synchrotron and inverse Compton radiation - have already been described for the case of the Crab PWN, but the Crab is far from the typical object. Understanding of the structure and evolution of PWN has advanced significantly over the past few years, in particular thanks to the high resolution X-ray imaging provided by *Chandra* (see Gaensler and Slane [104] for a detailed review). Initially, the PWN expands uniformly from the central pulsar, while at later stages the nebula may be confined and distorted by the reverse shock from the expanding supernova remnant (SNR).

At TeV energies, young PWN are usually still embedded within their parent SNR and are point-like, within the angular resolution of IACTs. They are positionally coincident with a bright X-ray synchrotron nebula powered by a pulsar with very high spin-down luminosity (e.g. G0.9+0.1 [105], HESS J1813-178 [106], G54.1+0.3 [107]). More evolved PWN, with ages  $> 10,000$  years, are usually much larger, and their TeV emission can be spatially resolved and mapped. The pulsar powering the nebula is often offset from the center of the TeV emission, probably for reasons related to density gradients in the medium surrounding the SNR [108]. Remarkably, the TeV nebulae are often two or three orders of magnitude larger than the corresponding X-ray PWN, and the TeV PWN sizes tend to increase with age, while the X-ray PWN sizes show the opposite trend. This can be understood as a result of the fact that the electron population which is responsible for the TeV inverse Compton flux has lower energies than the electrons which produce the X-ray synchrotron emission. They therefore cool more slowly, and survive for longer so, while the X-ray nebula is dominated by freshly accelerated particles, the TeV nebula can record the entire history of particle propagation away from the pulsar. A natural result of this is that the observed TeV spectrum should vary with distance from the pulsar. One of the best examples of this is HESS J1825-137, associated with the PWN of the pulsar PSRJ1826-1334 [109]. Figure 12 shows the spatially dependent spectra for this

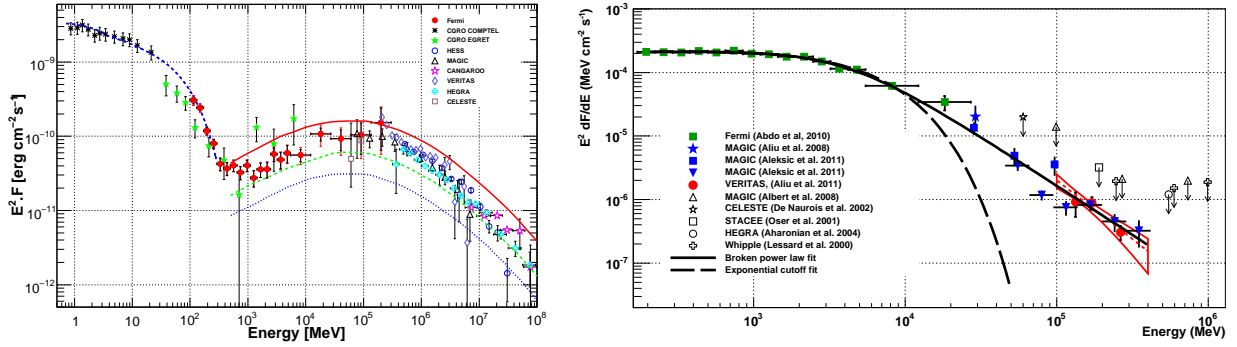


Figure 11: **Left:** The spectral energy distribution of the Crab Nebula from Abdo et al. [90]. Their fit to the synchrotron component is shown (blue dashed line), as well as inverse Compton spectra from Atoyan and Aharonian [97] for assumed magnetic field strengths of  $100 \mu\text{G}$  (solid red line),  $200 \mu\text{G}$  (dashed green line) and  $300 \mu\text{G}$  (dotted blue line). **Right:** High Energy spectrum of the Crab Pulsar. The black dashed line shows a fit of a power law with exponential cut-off to the *Fermi*-LAT data alone; the solid line shows a broken power law fit to the LAT and IACT data. The red dashed line and bowtie shows a power law fit to the VERITAS points alone. Figure courtesy of N. Otte (priv. comm.).

source, which softens with increasing distance from the pulsar. This is interpreted as the natural effect of both inverse Compton and synchrotron cooling of the electron population during propagation. A counter-example is the case of Vela-X [110, 111], in which no spectral variability is seen over the extended nebula, suggesting that cooling does not play an important role.

#### 5.4. Supernova Remnants

The search for the origin of the cosmic rays triggered the development of gamma-ray astronomy, and continues to motivate many gamma-ray observations. Chief among these is the study of supernova remnants, which are believed to efficiently accelerate particles at the shock front where the expanding SNR encounters the surrounding medium (e.g. [112]). This likely occurs through diffusive shock acceleration (first order Fermi acceleration), in which charged particles are reflected from magnetic inhomogeneities and repeatedly cross the shock front, gaining energy with each crossing (see e.g. [113, 114]). As well as plausibly providing enough energy to explain the observed Galactic cosmic ray population, this process naturally produces a power law distribution of particle energies with an index of  $\sim 2$ , which matches the cosmic ray spectrum (after accounting for diffusion and escape). In recent years, the importance of magnetic field amplification by the accelerated particles themselves has been increasingly recognised, and plays a particular role in explaining the existence of the highest energy Galactic cosmic rays, around the cosmic ray knee region (at  $\sim 3 \times 10^{15}$  eV).

The evidence for efficient leptonic acceleration in SNRs is now clearly established (e.g. [115]); however, the question of whether SNR are efficient hadron

accelerators is more difficult to answer. A definitive measurement would be the detection of high energy neutrinos from an SNR, but the expected fluxes are likely below the sensitivity thresholds of current neutrino observatories. Gamma-ray observations may provide the key, since the interactions of high energy nuclei with target material produce neutral pions, which decay immediately into gamma-rays. Disentangling the spectral signature of this process from other sources of gamma-ray emission (i.e. leptonic inverse Compton and bremsstrahlung processes) is difficult, but not impossible. Two classes of gamma-ray source are of interest for these studies: those which can be clearly associated with SNR shells, based on the gamma-ray morphology, and sources which are coincident with a massive volume of target material, such as molecular clouds.

The definitive association of gamma-ray emission with an SNR shell is often difficult to make, due to the presence of other potential counterparts, particularly PWN. A handful of shell-type SNRs have been unequivocally identified as gamma-ray sources by IACTs. This identification can be made on the basis of the observed shell morphology, (RXJ 1713.7-3946 [116], RXJ 0852.0-4622 (Vela Jr) [117], HESS J1731-3467 [118], SN1006 [119] and, possibly, RCW 86 [120]), or, in the case of Tycho's SNR [121], on the positional coincidence, coupled with the fact that the progenitor was a known Type Ia explosion, and so no compact object is present. Figure 13 shows the gamma-ray map for the first SNR shell to be resolved, RXJ 1713.7-3946. The recent addition of *Fermi*-LAT observations to the broadband spectrum of RXJ 1713.7-3946 [122] are consistent with a leptonic origin as the dominant mecha-

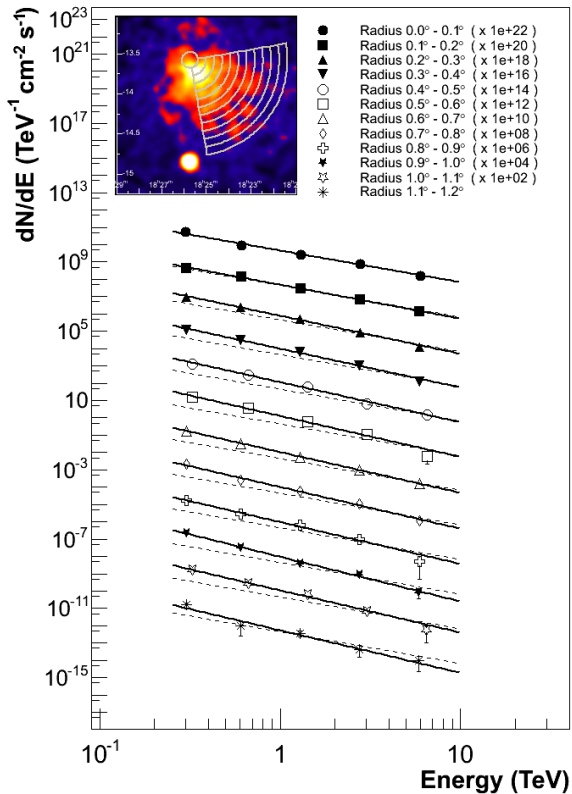


Figure 12: Inset: H.E.S.S. gamma-ray excess map for HESS J1825-137. The wedges show the radial regions with radii in steps of  $0.1^\circ$  in which the energy spectra were determined. The main figure shows the differential energy spectra for the regions illustrated in the inset, scaled by powers of 10 for the purpose of viewing. The spectrum for the analysis at the pulsar position is shown as a reference along with the other spectra as dashed line. Figure from [109]: see that paper for full details.

nism for the gamma-ray emission. A counter-example is illustrated by the spectrum in Figure 13, which corresponds to Tycho’s SNR. In this case, the fact that the broadband gamma-ray spectrum can be fit with a single hard power law from 500 MeV to 10 TeV favours a hadronic origin [123, 124]. This interpretation is not completely compelling, however, given the large statistical errors in the measurements, and the impact of various unknown parameters such as the SNR distance, and possible enhancements of the gamma-ray flux due to a nearby molecular cloud. Additionally, Atoyan and Dermer [125] describe a two-zone leptonic model which provides an acceptable spectral fit. Future measurements of the spectrum below 500 MeV, and deeper exposure at TeV energies, will further test the differing interpretations.

The intensity of gamma-ray emission due to hadronic

interactions depends upon the flux of high energy nuclei, and also upon the density of target material. Regions of high matter density (e.g. molecular clouds with densities  $> 100 \text{ cm}^{-3}$ ), situated close to sites of particle acceleration (such as SNRs), can therefore be expected to produce a large gamma-ray flux due to hadronic interactions. At TeV energies,  $\sim 10$  likely candidates for this process have been identified. The task of identification is complicated, both for the usual reasons of source confusion, and also because the evidence for a molecular cloud / SNR interaction is only definitive in those cases where the cloud morphology is visibly deformed by the expanding SNR, and/or where sites of hydroxyl (OH) maser emission indicate the presence of shocked molecular material. One of the best examples of this source class is the old remnant W28 [126]. H.E.S.S. observations of this region show four distinct sites of emission, with three of the four showing a resolvable angular extent ( $\sim 10'$ ). Each of the TeV sources is positionally coincident with a molecular cloud. Assuming that the TeV emission is due to hadronic cosmic rays interacting with the cloud material, the cosmic ray density is inferred to be a factor of 10 to 30 times greater than in the solar neighbourhood.

### 5.5. Star forming regions

The process of diffusive shock acceleration is not limited to supernova remnant shells. An alternative scenario invokes particle acceleration at the shock formed by the collision between the supersonic stellar winds of massive stars in close binary systems. Stellar winds may also become collectively important in large assemblies of massive stars. The combined effect of the stellar winds, coupled with the effect of multiple SNRs, results in an overall wind from the cluster which forms a giant *superbubble* in the interstellar medium. Particle acceleration can occur where the cluster wind interacts with the surrounding medium (e.g. [127]).

Massive star associations are naturally likely to host other potential source counterparts for TeV emission, such as compact object binary systems, individual supernova remnants and pulsar wind nebulae. A case in point is the young, open cluster Westerlund 2, containing the Wolf-Rayet binary system WR 20a. This was originally suggested as a plausible counterpart to the unidentified source HESS J1023-575, with the emission presumed to be connected to either the Wolf-Rayet binary, or the combined cluster wind [128]. A reassessment of this region, informed by a deeper H.E.S.S. exposure and results from *Fermi*-LAT, alters the picture [129]. The LAT detects an energetic pulsar, PSR J1022-5746, which drives a PWN which is bright in GeV



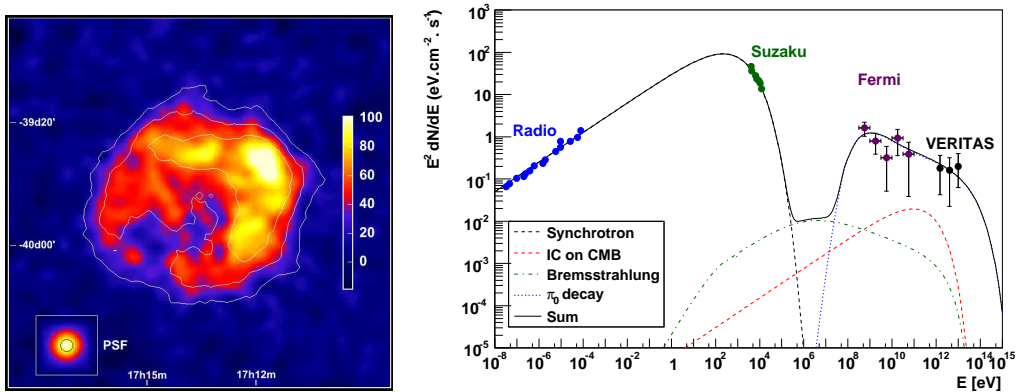


Figure 13: **Left:** H.E.S.S. map of gamma-ray excess events for RXJ 1713.7-3946 - the first SNR shell to be resolved at TeV energies. Figure from [116]. **Right:** The broadband SED of Tycho's SNR from [124], together with models for the various emission components (dominated by hadronic processes in the gamma-ray band). See paper for details.

gamma-rays [130]. Given the ubiquity of bright TeV PWN, this now seems the most likely explanation for the TeV source. A similar conclusion may arise for the first TeV source to be linked with a massive star association, TeV 2032+4130 (coincident with the Cyg OB2 association). In this case, the LAT pulsar (PSR J2032+4127) is sufficiently energetic to explain the TeV emission, although no PWN has been detected as yet.

Other unidentified sources which have been linked with massive star clusters and associations include HESS J1646-458 (Westerlund 1) [131], HESS J1614-518 (Pismis 22) [132], HESS J1848-018 (W43, which hosts Wolf-Rayet star WR121a) [133] and W49A [134], a massive star forming region. For all of these, however, the evidence that particle acceleration in stellar winds is the driving force behind the gamma-ray emission is not definitive (e.g. [135]).

### 5.6. Compact Object Binary Systems

Despite many early unconfirmed claims, the first definitive detection of a TeV gamma-ray binary system was not published until 2005. The population has grown slowly, and now consists of four clearly identified systems, plus marginal evidence for transient emission associated with Cyg X-1 [136]. The gamma-ray emission from binaries is believed to be powered either by accretion (most likely onto a black hole), or by a pulsar wind. In the case of accretion, particle acceleration takes place in relativistic jets (e.g. [137]). In the pulsar wind scenario, the acceleration occurs either in shocks where the pulsar wind encounters the circumstellar environment (e.g. [138]), or possibly within the pulsar wind zone itself [139]. The detection of Cyg X-1, if confirmed,

would be extremely important, since there is no doubt that this system hosts a black hole. This is in contrast to all of the other TeV binaries, in which the compact object is either known to be, or may be, a neutron star. Here we briefly summarize the results for each of the four well-studied objects.

**PSR B1259-63/LS 2883:** This was the first gamma-ray binary system to be firmly detected at TeV energies, and the first known variable VHE source in our Galaxy [140]. The system comprises a 48 ms pulsar orbiting a massive B2Ve companion. The orbit is highly eccentric ( $e = 0.87$ ), with a period of 3.4 years. The TeV emission exhibits two peaks, approximately 15 days before and after periastron. Various authors have attempted to explain the double bumped VHE lightcurve within a 'hadronic disk scenario', in which a circumstellar disk provides target material for accelerated hadrons, leading to  $\pi^0$  production and subsequent TeV gamma-ray emission [141, 142]. The 2007 H.E.S.S. observations disfavour this, since the onset of TeV emission occurs  $\sim 50$  days prior to periastron, well before interactions with the disk could be expected to play a significant role [143]. Leptonic scenarios have also been discussed in e.g. Kangulyan et al. [144].

The recent discovery of an extended and variable radio structure in PSR B1259-63/LS 2883 at phases far from periastron provides definitive evidence that non-accreting pulsars orbiting massive stars can produce variable and extended radio emission at AU scales [145]. This is important, since similar structures in LS 5039 and LS I +61°303, where the nature of the compact object is not certain, have been used to argue for the existence of jets driven by accretion onto a black



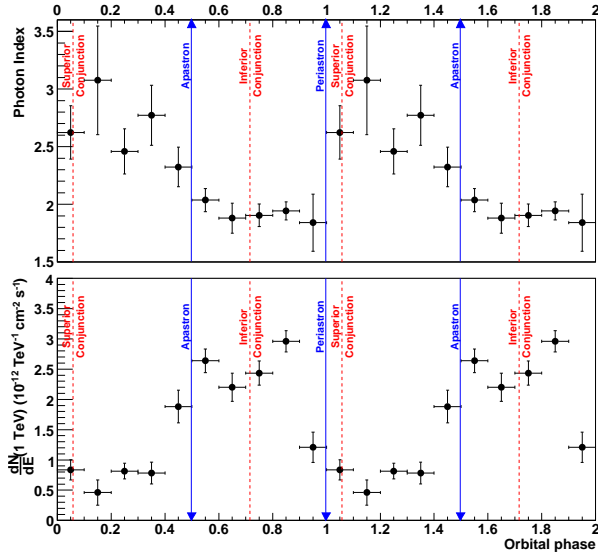


Figure 14: The H.E.S.S. flux (bottom) and photon index (top) for LS 5039 as a function of orbital phase. Figure from Aharonian et al. [146].

hole.

**LS 5039:** LS 5039 consists of a compact object, either neutron star or black hole, orbiting a massive O6.5V ( $\sim 23 M_{\odot}$ ) star in a 3.9 day orbit. Observations by H.E.S.S. in 2004 revealed that LS 5039 is a bright source of VHE gamma-rays [146]. Unlike PSR B1259-63 (and, to a lesser extent, LS I +61°303) LS 5039 is almost perfectly suited to TeV observations, with a short orbital period and a convenient declination angle, allowing sensitive observations at all phases over numerous orbits. The VHE emission measured by H.E.S.S. is modulated at the orbital period, peaking around inferior conjunction, when the compact object is closest to us and co-aligned with our line-of-sight (Figure 14). The spectrum is also orbitally modulated, appearing significantly harder around inferior conjunction ( $\Gamma = 1.85 \pm 0.06_{\text{stat}} \pm 0.1_{\text{sys}}$ ), but with an exponential cut-off at  $E_o = 8.7 \pm 2.0$  TeV. At GeV energies, the source is detected by *Fermi*-LAT at all orbital phases, with the emission peaking close to superior conjunction, in apparent anti-phase with the VHE results [147]. A sharp spectral cut-off at  $E_o = 1.9 \pm 0.5$  GeV is observed in the LAT data near superior conjunction, indicating that the VHE spectra cannot be simply a smooth extrapolation of the lower energy emission.

**LS I +61°303:** Similar to LS 5039, LS I +61°303 consists of a compact object, either neutron star or black hole, in this case orbiting a B0Ve star with a circumstellar disk ( $\sim 12.5 M_{\odot}$ ) in a 26.5 day orbit. The de-

tection of a variable VHE source at the location of LS I +61°303 with MAGIC [148], later confirmed by VERITAS [149], established this source as a gamma-ray binary. The object is now one of the most heavily observed locations in the VHE sky, with deep exposures by the two observatories spread over half a decade. Despite this, the VHE source is much less well-characterized than LS 5039, owing to its relatively weak VHE flux, and an inconvenient orbital period which closely matches the lunar cycle, making observations over all orbital phases almost impossible within a single observing season. VHE emission was originally detected close to apastron, between phases  $\phi = 0.5 - 0.8$ . In contrast to this, VHE observations between 2008 and 2010 showed that, at least during the orbits when the source was observed, the apastron flux was much lower than during the previous detections [150, 151]. The detection of TeV emission by VERITAS during a single episode close to superior conjunction complicates the picture even further. As with LS 5039, the *Fermi*-LAT GeV emission peaks closer to periastron, and the spectrum displays sharp cut-off, at  $E_o = 6.3 \pm 1.1$  GeV. Long term variability in the GeV band has also been observed [152].

**HESS J0632+057:** This TeV source was serendipitously detected during H.E.S.S. observations of the Monoceros Loop SNR region, and noted as a potential binary primarily because of its small angular extent [153]. Subsequent observations revealed it to be a variable TeV source [154], and co-located with a variable radio and X-ray source, at the position of a massive Be star, MWC 148 [155]. X-ray observations with Swift recently provided definitive proof of its binary nature, with the measurement of a  $321 \pm 5$  day periodicity in the lightcurve [156]. The TeV light curve displays a broad gamma-ray flare close to the X-ray maximum, with a duration of  $\sim 40$  days [157]. No GeV source has been detected.

A number of competing processes likely contribute to the variability observed in the gamma-ray binaries. In particular, the efficiency of inverse Compton gamma-ray production, as well that of VHE gamma-ray absorption (through pair production), changes as a function of orbital phase. This can go some way towards explaining the apparent phase shift between the GeV and TeV lightcurves, for example in the case of LS 5039. There are clearly other effects which contribute, however, as demonstrated by the long term instability of LS I +61°303. The sharp GeV cut-offs in these systems are also difficult to explain, and may indicate that the GeV and TeV emission components do not have the same origin.

A final comment should be reserved for the *Fermi*-LAT source 1 FGL J1018.6-5856, which was recently identified as a GeV binary system, with a period of  $16.58 \pm 0.04$  days [158]. This source resides in a complex region, coincident with the center of the SNR G284.3-1.8, and close to a LAT pulsar (at a distance of  $35'$ ). The extended, unidentified HESS source, HESS J1018-589, overlaps with the GeV binary location, and appears to consist of a point-like source overlaid on a diffuse structure [159]. While this is indicative of a new TeV binary there is, as yet, no evidence for variability in the point-like emission, making the identification still uncertain.

### 5.7. Globular Clusters

A single globular cluster, Terzan 5, has been suggested as the probable counterpart of a TeV source (HESS J1747-248) [160]. If the association is correct, the emission is likely related to the large population of millisecond pulsars in this cluster, which provide an injection source of relativistic leptons [161]. Inverse Compton gamma-ray photons result when these electrons upscatter low energy photons of the intense stellar radiation field. The H.E.S.S. source is extended, and slightly offset from the cluster core (although there is significant overlap). The probability of this being simply a chance positional coincidence is  $\sim 10^{-4}$ .

Globular clusters have also been favored targets in searches for dark matter particle annihilation signatures, since they may have been generated in dark matter mini-haloes before the formation of galaxies took place, and thus retain a significant dark matter component [162, 163]. Limits have been placed on NGC 6388, M15, Omega Centauri, 47 Tuc, M13, and M5 ([164], and references therein).

### 5.8. Unidentified objects

IACTs are able to locate point sources with reasonably good accuracy (typically  $\lesssim 1'$  for a moderately strong source). Extragalactic TeV sources can therefore usually be firmly identified with a single counterpart at other wavelengths. For Galactic sources, identification poses more of a problem, and around one third of the Galactic sources lack a firm identification. While the diffuse Galactic background emission, which dominates at GeV energies, is not significant, the TeV sources themselves are mostly extended, and can often be plausibly associated with multiple counterparts. PWN, in particular, often have their brightest TeV emission offset from the location of the parent pulsar or X-ray PWN, which may not yet have been detected (a number of new

energetic pulsars have been located in follow-up observations of unidentified TeV sources). In other cases, despite deep X-ray and radio follow-up observations, no reasonable counterpart has yet been found.

The unidentified Milagro sources also pose some interesting questions. While IACTs have identified sources associated with these objects, the TeV sources are typically much smaller in angular extent, and cannot account for the entire Milagro flux. One possible explanation for this is that there is a diffuse high energy component to the emission, which is difficult to resolve with IACTs, given their relatively small fields of view.

## 6. The Future

The field of ground-based gamma-ray astronomy has expanded dramatically over the past 10 years, but it is worth noting that the observatories currently operating are far from reaching the physical limits of the detection techniques. We therefore conclude this review with a brief discussion of some of the instrumental developments which can be expected over the next decade.

The IACTs currently operating have all made significant efforts to maintain, and improve, sensitivity since they were first commissioned. H.E.S.S. recoated the telescope mirrors, and successfully developed sophisticated analysis tools with which to exploit the data. VERITAS relocated their original prototype telescope to provide a more favorable array layout, halving the time required to detect a weak source. Most significantly, MAGIC added a second telescope of similar design to the first, providing a stereo pair with a baseline of 85 m. All of these observatories have further upgrade plans. Both MAGIC and VERITAS are implementing camera upgrades - in the case of VERITAS this involves the replacement of all of the camera PMTs with more sensitive, super-bialkali devices in summer 2012. H.E.S.S. are constructing H.E.S.S. II - the addition of a single large telescope, with  $600 \text{ m}^2$  mirror area, to the centre of the array. Figure 15 shows the telescope structure in November 2011. The mirrors and camera will be installed in the first half of 2012.

Novel approaches are also being pursued by many smaller projects. A particularly nice example of this is FACT (the First G-APD Cherenkov Telescope), which has recently demonstrated the application of Geiger-mode Avalanche Photodiodes for Cherenkov astronomy. The FACT telescope consists of a 1440-pixel G-APD camera at the focus of one of the original HEGRA telescopes. Geiger-APDs hold great promise as a potential replacement for PMTs, since they are robust, and offer much better photon conversion efficiency. Figure 16



Figure 15: The steel structure for the 600 m<sup>2</sup> H.E.S.S. II telescope. Mirrors and camera will be installed in the first half of 2012. (Note that the H.E.S.S. II telescope is located in between the two H.E.S.S. I telescopes shown in the image, not in the foreground). Figure courtesy of the H.E.S.S. collaboration <http://www.mpi-hd.mpg.de/hfm/HESS/>

shows some “first light” images from FACT. Other projects in development include GAW (Gamma Air Watch), MACE (Major Atmospheric Cerenkov Telescope Experiment) and LHASSO (Large High Altitude Air Shower Observatory). LHASSO is an ambitious project which will be located near the site of the ARGO-YBJ experiment in Tibet. It is planned to consist of four water Cherenkov detectors, two IACTs, three fluorescence telescopes and a large scintillator array.

For the particle detectors, the next stage in instrumentation is HAWC (the High Altitude Water Cherenkov Observatory). HAWC will consist of 300 individual water Cherenkov tanks, at an altitude of 4100 m in Mexico. The final array is expected to be 15 times more sensitive than Milagro, and will be a powerful tool for surveying, and for observations of transient phenomena. A prototype system is already in operation, and science operations will start in spring 2012, with completion of the full array expected in 2014.

The most ambitious future project is CTA (the Cherenkov Telescope Array). This is described in detail in [165]. Briefly, it comprises an array of imaging atmospheric Cherenkov telescopes covering  $\sim 1 \text{ km}^2$ , providing a factor of 5-10 improvement in sensitivity in the 100 GeV-10 TeV range, and extending the energy range both above and below these values. Both a northern and a southern site are envisaged, and the ar-

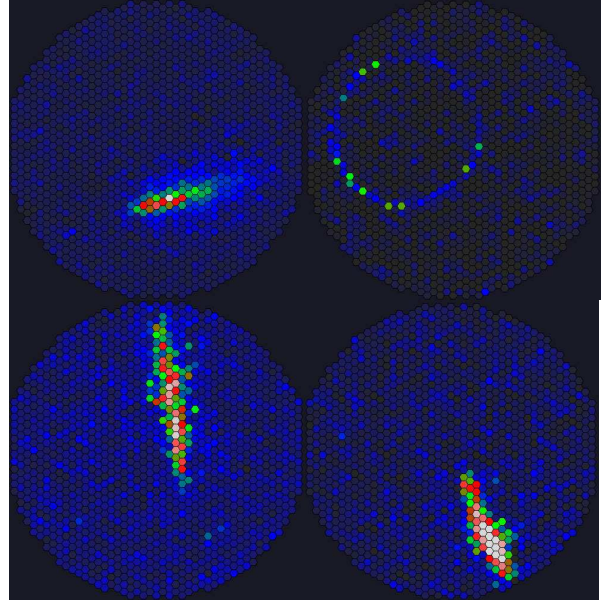


Figure 16: First light cosmic ray images from FACT (First G-APD Cherenkov Telescope). Four different events are shown; the upper right event shows the characteristic ring image produced by a local muon. The camera contains 1440 Geiger-mode avalanche photodiodes, installed on one of the original HEGRA telescopes at the Roque de los Muchachos on La Palma. Figure courtesy of the FACT collaboration <http://fact.ethz.ch/first>

ray will be operated as an open observatory. Multiple telescope designs are planned, including small (few m), medium (10 – 15 m) and large (20 – 30 m) diameter reflectors, as well as two-mirror telescope designs, such as the Schwarzschild-Couder [166].

In conclusion, TeV gamma-ray astronomy now describes a broad astronomical discipline which addresses a wide, and expanding, range of astrophysical topics. With planned instrumental developments, it is not unreasonable to expect the source catalogue to exceed 1000 objects within the next decade. Much of the TeV sky remains relatively unexplored. Less than  $\sim 10\%$  of the sky has been observed with  $\sim 10$  milliCrab sensitivity at 1 TeV, and the sensitive exposure to transient events and widely extended sources at these energies is much lower. The likelihood of continued exciting results is certain, both for the known sources and source classes, and for new discoveries.

## References

- [1] T. C. Weekes, et al., *ApJ* 342 (1989) 379–395.
- [2] J. A. Hinton, W. Hofmann, *ARA&A* 47 (2009) 523–565.
- [3] F. Aharonian, J. Buckley, T. Kifune, G. Siniis, *Reports on Progress in Physics* 71 (2008) 096901.

- [4] P. M. Chadwick, I. J. Latham, S. J. Nolan, *Journal of Physics G Nuclear Physics* 35 (2008) 033201.
- [5] F. A. Aharonian, *Very high energy cosmic gamma radiation: a crucial window on the extreme Universe*, River Edge, NJ: World Scientific Publishing, 2004.
- [6] P. Morrison, *Nuovo Cimento* 7 (1958) 858.
- [7] G. Cocconi, in: *Proc. International Cosmic Ray Conference, Moscow, 2 (1959)* 309.
- [8] W. Galbraith, J. V. Jelley, *Nature* 171 (1953) 349–350.
- [9] T. C. Weekes, K. E. Turver, in: R. D. Wills & B. Battrick (Ed.), *Recent Advances in Gamma-Ray Astronomy*, 124 (1977) 279.
- [10] A. M. Hillas, in: F. C. Jones (Ed.), *Proc. 19th International Cosmic Ray Conference, NASA Goddard Space Flight Center, 7 (1985)* 231.
- [11] M. Punch, et al., *Nature* 358 (1992) 477.
- [12] J. Quinn, et al., *ApJL* 456 (1996) L83.
- [13] A. Daum, et al., *Astroparticle Physics* 8 (1997) 1–11.
- [14] S. P. Wakely, D. Horan, in: Rogelio Caballero, Juan Carlos D’Olivo, Gustavo Medina-Tanco, Lukas Nellen, Federico A. Sanchez, Jos F. Valds-Galicia (Ed.), *Proc. 30th International Cosmic Ray Conference, Mérida, Yucatán, Mexico, 3 (2008)* 1341.
- [15] T. A. McKay, et al., *ApJ* 417 (1993) 742.
- [16] F. Aharonian, et al., *A&A* 390 (2002) 39–46.
- [17] A. A. Abdo, et al., *ApJL* 700 (2009) L127–L131.
- [18] A. A. Abdo, et al., *ApJL* 664 (2007) L91–L94.
- [19] Z. Cao, S. Z. Chen, for the ARGO-YBJ collaboration, *ArXiv e-prints*, 1110.1809 (2011).
- [20] M. Amenomori, et al., *ApJ* 692 (2009) 61–72.
- [21] L. Costamante, G. Ghisellini, *A&A* 384 (2002) 56–71.
- [22] A. A. Abdo, et al., *ApJ* 727 (2011) 129.
- [23] H. Krawczynski, et al., *ApJ* 601 (2004) 151–164.
- [24] F. A. Aharonian, *New Ast. Rev.* 5 (2000) 377–395.
- [25] H.E.S.S. Collaboration, *A&A* 520 (2010) A83.
- [26] J. A. Gaidos, et al., *Nature* 383 (1996) 319–320.
- [27] S. D. Biller, et al., *Physical Review Letters* 83 (1999) 2108–2111.
- [28] H.E.S.S. Collaboration, *Astroparticle Physics* 34 (2011) 738–747.
- [29] F. Aharonian, et al., *ApJL* 664 (2007) L71–L74.
- [30] J. Aleksić, et al., *ApJL* 730 (2011) L8.
- [31] S. J. Wagner, H.E.S.S. collaboration, in: *AAS/High Energy Astrophysics Division, Meeting #11 (2010)* #27.06.
- [32] J. Aleksić, et al., *A&A* 530 (2011) A4.
- [33] T. A. Rector, J. T. Stocke, E. S. Perlman, *ApJ* 516 (1999) 145–162.
- [34] A. Neronov, D. Semikoz, I. Vovk, *A&A* 519 (2010) L6.
- [35] J. Aleksić, et al., *ApJL* 723 (2010) L207–L212.
- [36] F. W. Stecker, O. C. de Jager, M. H. Salamon, *ApJL* 390 (1992) L49–L52.
- [37] F. Aharonian, et al., *Nature* 440 (2006) 1018–1021.
- [38] MAGIC Collaboration, *Science* 320 (2008) 1752.
- [39] M. R. Orr, F. Krennrich, E. Dwek, *ApJ* 733 (2011) 77.
- [40] F. A. Aharonian, P. S. Coppi, H. J. Voelk, *ApJL* 423 (1994) L5–L8.
- [41] S. Gabici, F. A. Aharonian, *Ap&SS* 309 (2007) 465–469.
- [42] D. Hooper, P. D. Serpico, *Physical Review Letters* 99 (2007) 231102.
- [43] A. Domínguez, M. A. Sánchez-Conde, F. Prada, *JCAP* 11 (2011) 20.
- [44] F. Tavecchio, G. Ghisellini, G. Bonnoli, L. Foschini, *MNRAS* 414 (2011) 3566–3576.
- [45] C. D. Dermer, et al., *ApJL* 733 (2011) L21.
- [46] F. Aharonian, et al., *A&A* 403 (2003) L1–L5.
- [47] F. Aharonian, et al., *Science* 314 (2006) 1424–1427.
- [48] V. A. Acciari, et al., *ApJ* 679 (2008) 397–403.
- [49] J. Albert, et al., *ApJL* 685 (2008) L23–L26.
- [50] A. Abramowski, et al., *ApJ* 746 (2012) 151.
- [51] V. A. Acciari, et al., *Science* 325 (2009) 444.
- [52] F. Aharonian, et al., *ApJL* 695 (2009) L40–L44.
- [53] Ł. Stawarz, F. Aharonian, S. Wagner, M. Ostrowski, *MNRAS* 371 (2006) 1705–1716.
- [54] S. Lombardi, et al., *ArXiv e-prints*, 1111.0143 (2011).
- [55] D. Hildebrand, et al., *ArXiv e-prints*, 1110.5358 (2011).
- [56] A. M. Brown, J. Adams, *MNRAS* 413 (2011) 2785–2790.
- [57] VERITAS Collaboration, *Nature* 462 (2009) 770–772.
- [58] F. Acero, et al., *Science* 326 (2009) 1080.
- [59] B. C. Lacki, T. A. Thompson, E. Quataert, A. Loeb, E. Waxman, *ApJ* 734 (2011) 107.
- [60] K. Mannheim, D. Elsässer, O. Tibolla, *ArXiv e-prints*, 1010.2185 (2010).
- [61] N. Komin, et al., in: *Proc. 32nd International Cosmic Ray Conference, Beijing, (2011)*, *Arxiv e-prints*, 1201.0639.
- [62] A. A. Abdo, et al., *A&A* 512 (2010) A7.
- [63] D. A. Williams, et al., in: *astro2010: The Astronomy and Astrophysics Decadal Survey, volume 2010 of Astronomy*, p. 316.
- [64] A. A. Abdo, et al., *Science* 323 (2009) 1688.
- [65] A. A. Abdo, et al., *ApJ* 707 (2009) 580–592.
- [66] V. A. Acciari, et al., *ApJ* 720 (2010) 1174–1180.
- [67] J. Aleksić, et al., *A&A* 517 (2010) A5.
- [68] F. Aharonian, et al., *A&A* 495 (2009) 505–512.
- [69] V. A. Acciari, et al., *ArXiv e-prints*, 1109.0050 (2011).
- [70] T. Aune, for the VERITAS Collaboration, *ArXiv e-prints*, 1111.1326 (2011).
- [71] T. A. Porter, R. P. Johnson, P. W. Graham, *ARA&A* 49 (2011) 155–194.
- [72] A. Abramowski, et al., *Physical Review Letters* 106 (2011) 161301.
- [73] M. Vivier, for the VERITAS collaboration, *ArXiv e-prints*, 1110.6615 (2011).
- [74] J. Aleksić, et al., *JCAP* 6 (2011) 35.
- [75] H. E. S. S. Collaboration, *Astroparticle Physics* 34 (2011) 608–616.
- [76] F. Aharonian, et al., *ApJ* 691 (2009) 175–181.
- [77] F. Aharonian, et al., *Astroparticle Physics* 29 (2008) 55–62.
- [78] F. Aharonian, et al., *ApJ* 636 (2006) 777–797.
- [79] H. Gast, et al., in: *Proc. 32nd International Cosmic Ray Conference, Beijing, (2011)*.
- [80] K. Tsuchiya, et al., *ApJL* 606 (2004) L115–L118.
- [81] K. Kosack, et al., *ApJL* 608 (2004) L97–L100.
- [82] J. Albert, et al., *ApJL* 638 (2006) L101–L104.
- [83] F. Aharonian, et al., *Physical Review Letters* 97 (2006) 221102.
- [84] F. Aharonian, et al., *Nature* 439 (2006) 695–698.
- [85] F. Aharonian, et al., *A&A* 503 (2009) 817–825.
- [86] F. Acero, et al., *MNRAS* 402 (2010) 1877–1882.
- [87] C. F. Kennel, F. V. Coroniti, *ApJ* 283 (1984) 710–730.
- [88] O. C. de Jager, et al., *ApJ* 457 (1996) 253.
- [89] A. A. Abdo, et al., *Science* 331 (2011) 739.
- [90] A. A. Abdo, et al., *ApJ* 708 (2010) 1254–1267.
- [91] L. Kuiper, et al., *A&A* 378 (2001) 918–935.
- [92] E. Aliu, et al., *Science* 322 (2008) 1221.
- [93] A. P. S. Tang, J. Takata, J. J. Jia, K. S. Cheng, *ApJ* 676 (2008) 562–572.
- [94] E. Aliu, et al., *Science* 334 (2011) 69.
- [95] J. Aleksić, et al., *ApJ* 742 (2011) 43.
- [96] T. Y. Saito, for the MAGIC collaboration, *ArXiv e-prints*, 1109.6100 (2011).
- [97] A. M. Atayan, F. A. Aharonian, *MNRAS* 278 (1996) 525–541.
- [98] E. Striani, et al., *ApJL* 741 (2011) L5.
- [99] C. A. Wilson-Hodge, et al., *ApJL* 727 (2011) L40.

- [100] G. Di Sciascio, for the ARGO-YBJ Collaboration, ArXiv e-prints, 1107.3404 (2011).
- [101] E. de Oña Wilhelmi, in: M. Burgay, N. D’Amico, P. Esposito, A. Pellizzoni, & A. Possenti (Ed.), American Institute of Physics Conference Series, 1357 (2011) 213-220, pp. 213–220.
- [102] O. Kargaltsev, G. G. Pavlov, X-ray Astronomy 2009; Present Status, Multi-Wavelength Approach and Future Perspectives 1248 (2010) 25–28.
- [103] P. Slane, in: D. F. Torres & N. Rea (Ed.), High-Energy Emission from Pulsars and their Systems, Astrophysics and Space Science Proceedings (2011) 373.
- [104] B. M. Gaensler, P. O. Slane, ARA&A 44 (2006) 17–47.
- [105] F. Aharonian, et al., A&A 432 (2005) L25–L29.
- [106] F. Aharonian, et al., Science 307 (2005) 1938–1942.
- [107] V. A. Acciari, et al., ApJL 719 (2010) L69–L73.
- [108] J. M. Blondin, R. A. Chevalier, D. M. Frierson, ApJ 563 (2001) 806–815.
- [109] F. Aharonian, et al., A&A 460 (2006) 365–374.
- [110] F. Aharonian, et al., A&A 448 (2006) L43–L47.
- [111] J. A. Hinton, S. Funk, R. D. Parsons, S. Ohm, ApJL 743 (2011) L7.
- [112] L. O. Drury, F. A. Aharonian, H. J. Voelk, A&A 287 (1994) 959–971.
- [113] M. A. Malkov, L. O’C Drury, Reports on Progress in Physics 64 (2001) 429–481.
- [114] R. Blandford, D. Eichler, Phys. Rep. 154 (1987) 1–75.
- [115] Y. Uchiyama, et al., Nature 449 (2007) 576–578.
- [116] F. Aharonian, et al., A&A 449 (2006) 223–242.
- [117] F. Aharonian, et al., ApJ 661 (2007) 236–249.
- [118] A. Abramowski, et al., A&A 531 (2011) A81.
- [119] F. Acero, et al., A&A 516 (2010) A62.
- [120] F. Aharonian, et al., ApJ 692 (2009) 1500–1505.
- [121] V. A. Acciari, et al., ApJL 730 (2011) L20.
- [122] A. A. Abdo, et al., ApJ 734 (2011) 28.
- [123] G. Morlino, D. Caprioli, ArXiv e-prints, 1105.6342 (2011).
- [124] F. Giordano, et al., ApJL 744 (2012) L2.
- [125] A. Atayan, C. Dermer, ArXiv e-prints, 1111.4175 (2011).
- [126] F. Aharonian, et al., A&A 481 (2008) 401–410.
- [127] Y. Butt, Nature 460 (2009) 701–704.
- [128] F. Aharonian, et al., A&A 467 (2007) 1075–1080.
- [129] H.E.S.S. Collaboration, A&A 525 (2011) A46.
- [130] M. Ackermann, et al., ApJ 726 (2011) 35.
- [131] H.E.S.S. Collaboration, ArXiv e-prints, 1111.2043 (2011).
- [132] S. Ohm, et al., in: J. Martí, P. L. Luque-Escamilla, & J. A. Combi (Ed.), Proc. High Energy Phenomena in Massive Stars, Astronomical Society of the Pacific Conference Series, 422 (2010) 265.
- [133] R. C. G. Chaves, M. Renaud, M. Lemoine-Goumard, P. Goret, in: F. A. Aharonian, W. Hofmann, & F. Rieger (Ed.), American Institute of Physics Conference Series, 1085 (2008) 372-375.
- [134] F. Brun, for the H. E. S. S. Collaboration, Proc. of the 25th TEXAS Symposium on Relativistic Astrophysics, ArXiv e-prints, 1104.5003 (2011).
- [135] M. Lemoine-Goumard, et al., ArXiv e-prints, 1109.4733 (2011).
- [136] J. Albert, et al., ApJL 665 (2007) L51–L54.
- [137] V. Bosch-Ramon, D. Khangulyan, International Journal of Modern Physics D 18 (2009) 347–387.
- [138] G. Dubus, A&A 456 (2006) 801–817.
- [139] A. Sierpowska-Bartosik, D. F. Torres, Astroparticle Physics 30 (2008) 239–263.
- [140] F. Aharonian, et al., A&A 442 (2005) 1–10.
- [141] A. Kawachi, et al., ApJ 607 (2004) 949–958.
- [142] M. Chernyakova, et al., MNRAS 367 (2006) 1201–1208.
- [143] F. Aharonian, et al., A&A 507 (2009) 389–396.
- [144] D. Khangulyan, S. Hnatic, F. Aharonian, S. Bogovalov, MNRAS 380 (2007) 320–330.
- [145] J. Moldón, S. Johnston, M. Ribó, J. M. Paredes, A. T. Deller, ApJL 732 (2011) L10.
- [146] F. Aharonian, et al., A&A 460 (2006) 743–749.
- [147] A. A. Abdo, et al., ApJL 706 (2009) L56–L61.
- [148] J. Albert, et al., ApJ 693 (2009) 303–310.
- [149] V. A. e. a. Acciari, ApJ 679 (2008) 1427–1432.
- [150] V. A. Acciari, et al., ApJ 738 (2011) 3.
- [151] MAGIC Collaboration, ArXiv e-prints, 1111.6572 (2011).
- [152] D. Hadasch, D. F. Torres, T. Tanaka, R. H. D. Corbet, A. B. Hill, R. Dubois, G. Dubus, T. Glanzman, S. Corbel, J. Li, Y. P. Chen, S. Zhang, G. A. Caliandro, M. Kerr, J. L. Richards, W. Max-Moerbeck, A. Readhead, G. Pooley, ArXiv e-prints, 1202.1866 (2012).
- [153] F. A. Aharonian, et al., A&A 469 (2007) L1–L4.
- [154] V. A. Acciari, et al., ApJL 698 (2009) L94–L97.
- [155] J. A. Hinton, et al., ApJL 690 (2009) L101–L104.
- [156] S. D. Bongiorno, et al., ApJL 737 (2011) L11.
- [157] G. Maier, for the VERITAS Collaboration, J. Skilton, for the H.E.S.S. Collaboration, ArXiv e-prints, 1111.2155 (2011).
- [158] R. H. D. Corbet, et al., The Astronomer’s Telegram 3221 (2011) 1.
- [159] E. de Oña Wilhelmi, et al., in: Proc. 38th COSPAR Scientific Assembly, Bremen, Germany, 38, (2010) 2803.
- [160] W. Domainko, et al., in: Proc. 32nd International Cosmic Ray Conference, Beijing, (2011), Arxiv e-prints, 1112.4974.
- [161] C. Venter, O. C. De Jager, A.-C. Clapson, ApJL 696 (2009) L52–L55.
- [162] E. Komatsu, et al., ApJS 180 (2009) 330–376.
- [163] M. Wood, et al., ApJ 678 (2008) 594–605.
- [164] A. Abramowski, et al., ApJ 735 (2011) 12.
- [165] M. Actis, et al., Experimental Astronomy (2011) 121.
- [166] V. V. Vassiliev, S. J. Fegan, in: Rogelio Caballero, Juan Carlos D’Olivo, Gustavo Medina-Tanco, Lukas Nellen, Federico A. Sanchez, Jos F. Valds-Galicia (Ed.), Proc. 30th International Cosmic Ray Conference, Mérida, Yucatán, Mexico, 3 (2008) 1445-1448.